Graphical Means to Analyze and Visualize Vehicle Handling Behaviour

Joop P. Pauwelussen
HAN University
Mobility Technology Research
P.O. Box 2217, 6802 CE Arnhem, The Netherlands
e-mail: joop.pauwelussen@han.nl

ABSTRACT

Present developments in intelligent vehicle performance and active chassis control rely to a large extent on basic vehicle dynamics, where for the analysis of extreme vehicle behaviour the nonlinear axle characteristics have to be taken into account.
Smart vehicle analysis such as through multi-body tools, require multidisciplinary co-operation between experts from different backgrounds, such as communication technology, control engineering, electronics and human factors, with each of them necessarily having an understanding of vehicle dynamics. It is still a wonder that, with such a variety of skills, so many active chassis control systems reach the market successfully.
This fundamental understanding is often overlooked because of the large amount of output as a result of a sometimes too detailed analysis. On the other hand, it doesn't need an in depth knowledge of the basic vehicle dynamics equations, but can be obtained through graphical means with the data extracted from these simulation analyses. There are three different ways to graphically visualize the performance behaviour of a vehicle in relationship with vehicle and tyre parameters, with vehicle speed and steering input. Each of these graphical analysis tools will be treated in the paper and supported through simulation experiments. A first approach is given by the phase plane expressions, which illustrates the local and global vehicle performance near stationary points and in which areas can be identified related to this possible extreme performance. Quite a detailed treatment of this approach was originally given by Guo et. al. An understanding of these phase plane graphs is important in the discussion of vehicle response as preferred by the driver. A second well known approach is that of the handling diagram, originally introduced by Pacejka and extended for commercial vehicles with complex axle configurations by Winkler. This diagram is useful to identify stable and unstable stationary points, in relationship to different full nonlinear axle characteristics. It illustrates the relationship between steering, speed and road curvature, and it gives a basis to yaw-stability of road vehicles, with the global stability performance further illustrated by the phase plane diagrams, referred to before.
Finally, we will introduce a so-called stability diagram showing not only the stability (or lack of stability) of the vehicle performance but also the type of (in-)stability in dependence of the actual axle characteristics and vehicle speed. This refers to oscillatory or non-oscillatory limit behaviour, under- and oversteer and excessive understeer behaviour of road vehicles.
The paper will discuss the use of these graphical means with reference to practical vehicle dynamics analysis.

1. INTRODUCTION

Vehicle analysis can be carried out at different levels of complexity. One might start with the well-known one-track bicycle model, or one might start with a rather complex multi-body model including many details of the design. In this last case, one usually tries to validate the model based on vehicle tests like steady state cornering, step-steer or ramp-steer manoeuvring, random steer test, braking in a turn, etc. The performance as derived from such tests is to a large extent related to the basis vehicle characteristics which can be modelled by rather simple models such as the one-track model mentioned above. One is thus faced with the problem of having many degrees of freedom to be judged and/or many vehicle parameters to be tuned based on tests, the results of which can be interpreted through a limited amount of very essential overall vehicle properties.

It therefore makes sense to build an understanding of vehicle performance on simple models first and only then extend the model complexity, using the simple models in the validation process. In other words, if the overall vehicle characteristics are not validated properly, it makes no sense to examine vehicle or vehicle component performance in more detail.

But even with the more simple models, the resulting mathematics may be rather complex and difficult to use for interpretation of vehicle performance, especially in case of nonlinear tyre characteristics (limit behaviour). For this reason, various graphical tools have been developed in the past, supporting the researcher or vehicle engineer in this interpretation. Diagrams turn out to be remembered more easily, and to be applied quicker than going through a rigorous mathematical analysis all the time.
This paper deals with three of such graphical tools, the phase plane approach, the handling diagram and the so-called stability diagram.
The practical use of these tools is indicated in table 1 below.

Phase plane analysis (see for example Sachs, Pacejka, Guo, Smakman,..)	Expression of solution curves in terms of the vehicle states, with direct indication of cornering energy, steady state solutions, local and global stability, overshoot phenomena and related damping (underdamped, overdamped), position of pole of yaw rotation, interpretation of axle slipangles
Handling diagram (Pacejka, Winkler,..)	Clarifying the occurrence of steady state solutions in relationship with input parameters such as steering angle, path curvature, vehicle speed and the vehicle nonlinear axle characteristics. Interpretation of local and global stability with respect to these input parameters, under- and oversteer performance. Especially the direct relationship of stability with the nonlinear axle characteristics is visualized using this diagram.
Stability diagram	This diagram, not published before, visualizes the local vehicle performance near the steady state conditions in relationship with the separate nonlinear normalized axle characteristics near these points, the vehicle speed and the wheelbase. Stability for oversteer or excessive understeer conditions is graphically presented here in a convenient way, including indication of oscillatory or non-oscillatory limit behaviour.

Table 1.: Practical use of graphical tools to interpret vehicle handling performance

Each of these tools is treated in more detail in sections 2, 3 and 4 respectively, with a discussion on the combined use in section 5.

2. PHASE PLANE REPRESENTATION

All of the analyses, reviewed in this paper, are based on the single track vehicle model, describing vehicle handling behaviour neglecting roll as well as drive- and brake forces. This means that either small friction coefficients are assumed between tyre and road, or a centre of gravity of the vehicle being low relative to the vehicle track width. With these assumptions, both the front and rear wheels can be taken as one system, with an overall lateral force, aligning torque, and slip angle obtained from the combined effect of left en right wheel. It means that tyre characteristics are replaced by axle characteristics.
The slip angles for the front and rear axle are denoted by α_1 and α_2 . The total lateral forces for front and rear axle are denoted by F_{y1} and F_{y2}, respectively. The aligning torques will be disregarded. The vehicle

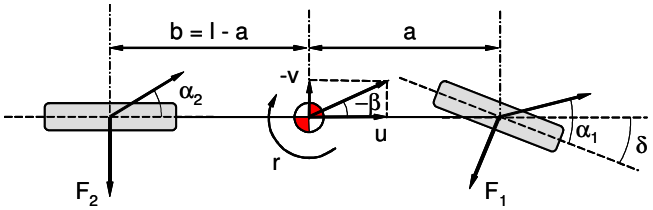

Fig.: 1.: Single track vehicle model

centre of gravity (c.o.g.) is positioned between both axles, at distances a and b from front and rear axle, respectively. The horizontal behaviour of the vehicle is described by a lateral velocity v at the c.o.g., a forward velocity u, a yaw rate r and a bodyslip angle β.
This leads to the following well known equations (for small β):

$$m(\dot{v} + u.r) = m.u(\dot{\beta} + r) = F_{y1} + F_{y2}$$
$$J_z.\dot{r} = a.F_{y1} - b.F_{y2} \qquad (1)$$

with vehicle mass m, and J_z the polar moment of inertia in z-direction (yaw moment of inertia), with the tyre forces depending on the slip angles in a nonlinear way (see also figure 2):

$$F_{y1} = F_{y1}(\alpha_1) \quad \text{and} \quad F_{y2} = F_{y2}(\alpha_2) \qquad (2)$$

The slipangles can be expressed in lateral speed and yawrate according to:

$$\alpha_1 = \delta - \frac{v + ar}{u} \;; \qquad \alpha_2 = -\frac{v - br}{u} \qquad (3)$$

In its most general form, system (1) can be written as:

$$\frac{d\,\underline{y}}{dt} = F(\underline{y}) \;; t > 0$$

where we write:

$$\underline{y} = \begin{pmatrix} y_1 \\ y_2 \end{pmatrix} \;; \quad \underline{y} : [0, \infty) \rightarrow R^2$$

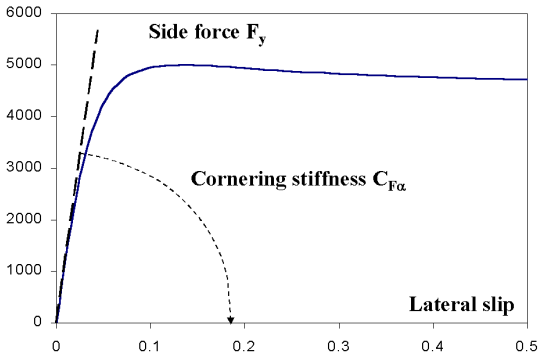

Fig.: 2.: Lateral force vs. slip angle

The two states y_1, y_2, plotted in a single diagram produce the so-called **phase plane**. The dynamic behaviour of the non-linear system can then be represented graphically in this phase-plane by a curve, denoted as a **phase curve** or **trajectory**.
The state-vector $\underline{y}$ can be chosen in different ways. One would choose $\underline{y} = (v, r.\rho/V)^T$, following (1), with ρ the radius of gyration defined by

$$J_z. = m.\rho^2$$

and the total vehicle speed V. Guo refers to this phase plane as the **energy phase plane** for reasons made clear below. Replacing (v, r) by the slip angles according to (3) one may choose $\underline{y} = (\alpha_1, \alpha_2)^T$. This second alternative has the advantage that these states are the key variables in the non-linear right-hand side of (1), allowing results that can be directly related to yaw-instability. See [3] for an interpretation of certain isoclines (curves in the phase plane intersecting trajectories at points with a specific slope) in this case. Smakman [5]

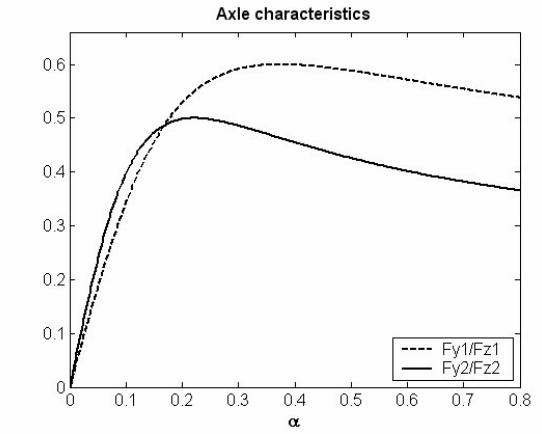

Fig.: 3.: Normalized axle characteristics

was interested in reference regions in the plane span by the bodyslip angle and bodyslip angle rate. He exploited the fact that small bodyslip angle is one of the criteria of good handling and he defined these preferred regions for his design of integrated control of slip (wheel-by-wheel braking) and active suspension.
For illustration, the three different phase plane presentations are shown in figure 4, for the normalized axle characteristics as depicted in figure 3 (lateral force, divided by the axle load), for constant steering angle 2^o and vehicle speed of 70 km/h.

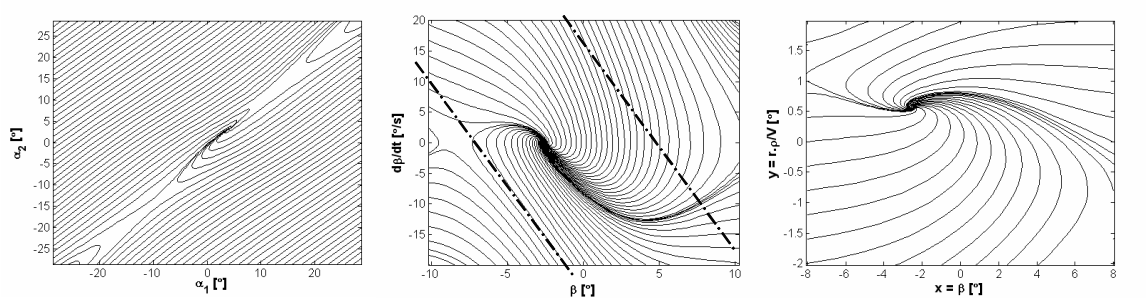

Fig. 4.: Phase plane representations according to Pacejka, Smakman, Guo

One observes three singular points in the outmost left picture, with the centre one being stable (attracting the trajectories). Trajectories being slightly apart from the line

$$\alpha_1 - \alpha_2 = \delta - \frac{l}{R} \tag{4}$$

for radius of curvature R and wheelbase l, tend not to approach this stable stationary solution, hence corresponding to a vehicle being lost in excessive yawing without additional steering control. A similar unstable behaviour is shown in the centre plot in the lower left corner. The area between the straight lines guarantees stability, and might be used as a preferred area for smooth vehicle performance. Finally, the right-hand plot shows trajectories moving oscillatory towards the steady state conditions. Points outside of the plot may still result in instabilities.

Let us focus on this final representation, being extensively studied by Guo [1], and list the various possible interpretations of trajectories as presented in [1]. First of all, one may observe that the cornering kinetic energy T_c can be expressed in terms of the vehicle states and the translational kinetic energy T_t as:

$$T_c = T_t.\left[\beta^2 + \left(\frac{r.\rho}{V}\right)^2\right]$$

Hence, the distance of trajectory points to the origin describes the square root of the normalised cornering energy as shown in figure 5, showing solution curves for two different ramp steer inputs. Observe the vortex at each curve, ending in the singular point corresponding to steady state vehicle performance, similar to the third plot in figure 4.

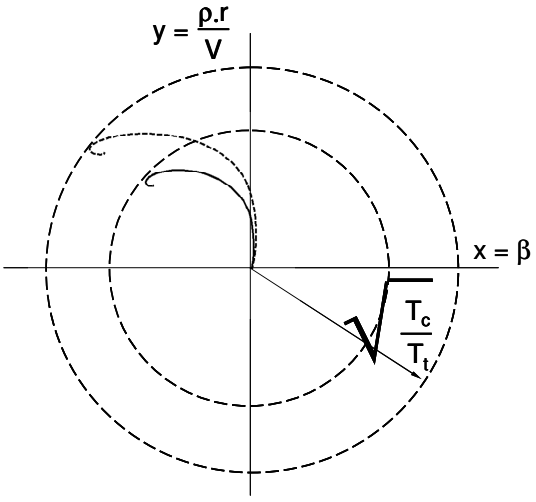

Fig. 5.: Energy phase plane

According to Guo in [1], this energy phase plane also allows for graphical interpretation of the slip angles. The expressions (3) for the slip angles for both axles, imply that the families of straight lines x

+ (a/ρ).y = const. and x - (b/ρ).y = const. correspond to constant values of α_1 - δ and α_2, being the angles of orientation of the local speed at front and rear axle, relative to the vehicle forward direction. These lines are shown in the energy phase plane in figure 6 for steady state steering angle $\delta = 4^o$ (with solution curve again corresponding to a ramp steer response) and a certain combination of axle characteristics. Intersections of these lines through any point of the trajectory with the x-axis result in both slipangles, as shown in figure 6. This figure also shows that as soon as the maximum steering angle is reached, the front slip angle is exceeded by the steering angle at the front axle, after which it increases again beyond the steering angle. The rear slipangle increases all the way, except for the area where the yawrate shows an overshoot. The distance between steering angle (first increasing and then constant) and front slipangle will first increase and then decrease. To illustrate this in time, the resulting slipangles for a rampsteer input are shown versus time in figure 7.

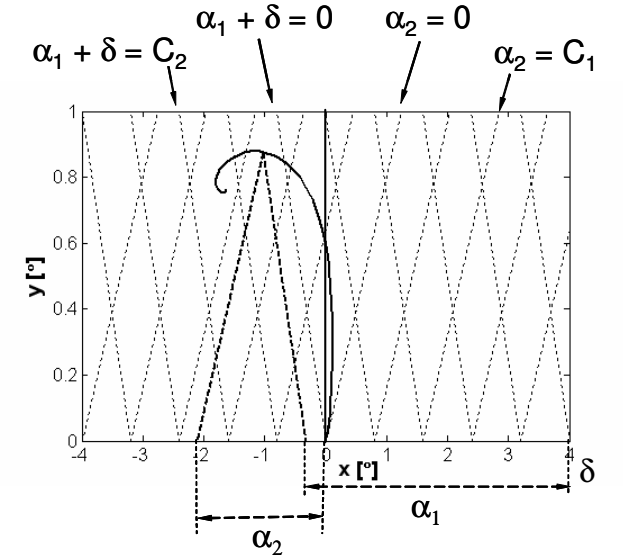

Fig. 6.: Front and rear slip angles.

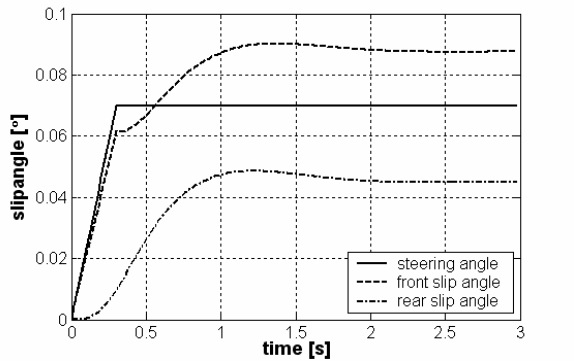

Fig. 7.: Slip angles, ramp steer input

Along the lines α_1 - δ = constant, the yawrate is increasing and the bodyslip angle is decreasing (in absolute sense). Consequently, the vehicle tends to obtain a spin motion. In the same way, along the lines α_2 = constant, the vehicle obtains a drift motion (larger bodyslip with decreasing yawrate).

Other observations are that the y-coordinate corresponds to the path curvature κ_{IC}:

$$y = \frac{\rho.r}{V} = \frac{\rho}{R_{IC}} = \rho.\kappa_{IC}$$

with turn radius R_{IC}, and that the cotangent of the argument of any point in the energy phase plane can be interpreted as the rotating length λ

$$\lambda = \rho.\frac{x}{y}$$

defined as the distance between the vehicle c.o.g. and the projection of the centre of rotation of the vehicle central plane through the axle centres, see figure 8.
For any point P (x, y) on a given trajectory, it is now easy to find the instant momentary pole of the vehicle planar motion from:

$$R_{IC} = \frac{\rho}{y};\ \lambda = \rho.\frac{x}{y}$$

In the first quadrant, the pole will be somewhat behind the vehicle c.o.g. whereas in the second quadrant, it will be somewhat in front of the vehicle c.o.g.

With the trajectory moving upward, the yawrate increases without significant change in bodyslip angle, i.e. the radius of curvature is decreasing and the vehicle is moving into a steady state curve, possibly in the shape of a vortex. Similarly, with the trajectory moving upward, the vehicle is heading for a larger curve radius.

.

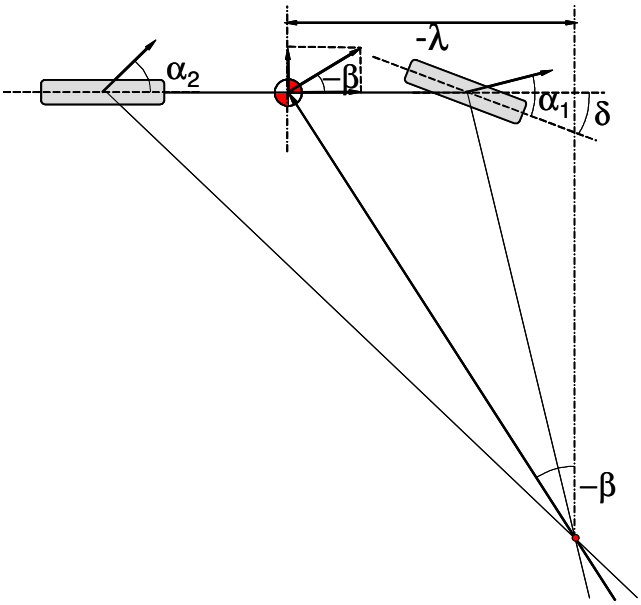

Fig. 8.: Rotating length and momentary pole of rotation

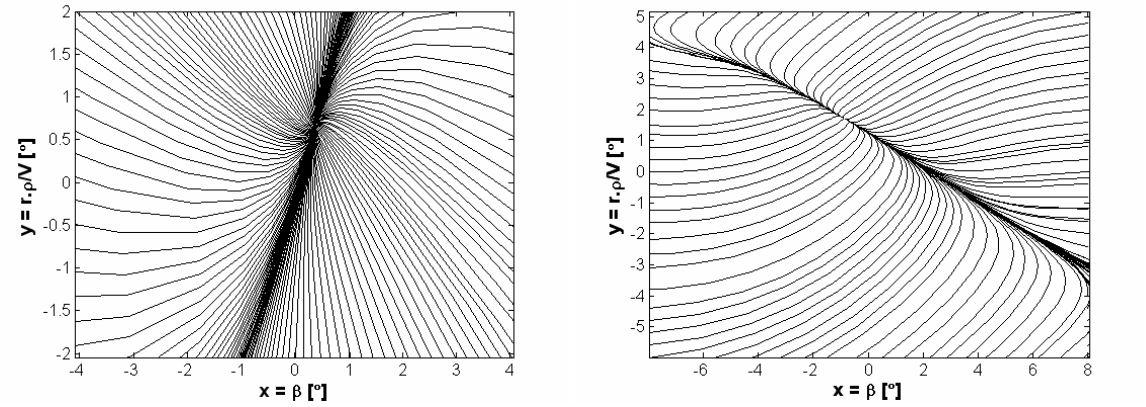

Fig. 9.: Energy phase plane respresentations for an understeered vehicle at low speed (left) and a stable oversteered vehicle

It is clear that the shape of the vortex near the steady state point defines the overshoot in both bodyslip angle and yawrate. As we know, such overshoot is not present for all possible situations. For example, a stable oversteered vehicle (velocity not exceeding the critical speed) or an understeered vehicle with low speed will approach the ciritical point directly, without spiralling around it first. For illustration, these two cases are shown in figure 9. We'll address these separate cases in section 4 in more detail. Note that the steady state value for the bodyslip angle β for the low speed understeer case remains positive.

We close this section with an outline of the different octants I-1, I-2, II-1,…,IV-2 formed by the four quadrants I, II, III, IV, with each of them divided further by the diagonal lines $\alpha_1 + \delta = 0$ and $\alpha_2 = 0$, see figure 6 and figure 10. We refer to [1] for further details.

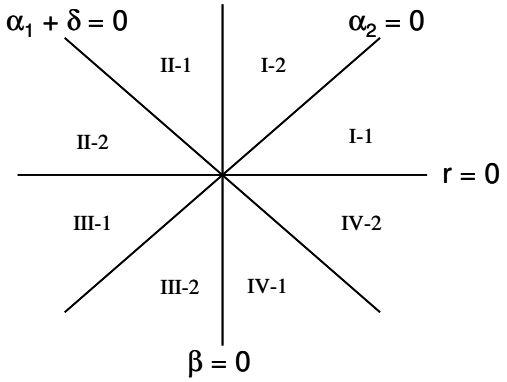

Fig. 10.: The eight zones in the energy phase plane

For a positive steering angle input, the phase plane trajectory will remain in quadrants I and II unless the vehicle becomes unstable. Just at the border of these two quadrants, the bodyslip angle changes sign. The quadrants III and IV are just similar to quadrant I and II, but for negative steering angle (and negative yawrate r). Within the zone, consisting of I-2 and II-1, the rotating length λ lies between both axle positions. Outside this zone within the first and second quadrant, the momentary pole of rotation has been moved further away in either the forward direction or the rearward direction, corresponding to the vehicle motion.
These observations are summarized in table 2, below.

Octant	Front slipangle	Rear slipangle	Rotating length	Bodyslip angle	Yawrate
I-1	$\geq \delta$	≤ 0	$\geq b$	≥ 0	≥ 0
I-2	$\geq \delta$	≥ 0	$0 \leq \lambda \leq b$	≥ 0	≥ 0
II-1	$\geq \delta$	≥ 0	$-a \leq \lambda \leq 0$	≤ 0	≥ 0
II-2	$\leq \delta$	≥ 0	$\leq -a$	≤ 0	≥ 0
III-1	$\leq \delta$	≥ 0	$\geq b$	≤ 0	≤ 0
III-2	$\leq \delta$	≤ 0	$0 \leq \lambda \leq b$	≤ 0	≤ 0
IV-1	$\leq \delta$	≤ 0	$-a \leq \lambda \leq 0$	≥ 0	≤ 0
IV-2	$\geq \delta$	≤ 0	$\leq -a$	≥ 0	≤ 0

Table 2. : The eight zones in the energy phase plane

3. HANDLING DIAGRAM

For further interpretation of these energy phaseplane representations of vehicle behaviour, we need some tool to illustrate the occurrence of steady state solutions and their stability, in terms of changing axle characteristics, input steering angle δ and vehicle forward speed V. Such a tool exists and is referred to as the **handling diagram**, see [3].
Following (1), steady state solutions of the one-track vehicle model satisfy

$$\frac{F_{y1}(\alpha_1)}{F_{z1}} = \frac{F_{y2}(\alpha_2)}{F_{z2}} = \frac{u.r}{g} = \frac{u^2}{gR} = \frac{K}{mg} \quad (=a_y \text{ in g's})$$

with total centrifugal force K=m.u.r, acceleration of gravity g and path radius $R = R_{IC}$.
Hence, the normalised axle characteristics (lateral force, divided by the axle load) front and aft coincide:

$$f_{y1}(\alpha_1) = f_{y2}(\alpha_2)$$

The lateral acceleration K/mg (in g) depends on the relative path curvature (a+b)/R = l/R in a linear sense:

$$a_y(g) = \frac{K}{mg} = \frac{u.r}{g} = \frac{u^2}{g.l}.\frac{l}{R} \tag{5}$$

For linear axles with cornering stiffnesses C_{F1} and C_{F2} respectively, it is well known that the vehicle understeer/oversteer performance can be described by the following relationshp:

$$\left[\frac{F_{z1}}{C_{F1}} - \frac{F_{z2}}{C_{F2}}\right].\frac{u^2}{g.R} \equiv \eta.\frac{u^2}{g.R} = \eta.a_y(g) = \alpha_1 - \alpha_2 = \delta - \frac{l}{R} \tag{6}$$

with coefficient η, referred to as understeer gradient. For such a linear vehicle, the definitions of understeer behaviour:

1. A vehicle is understeered if the steering angle has to be increased for increasing vehicle forward speed to negotiate the same curve.
2. A vehicle is understeered if the front axle slip angle exceeds the rear axle slip angle under steady state conditions: $\alpha_1 > \alpha_2$.
3. A vehicle is understeered if the understeer gradient $\eta>0$, i.e. the normalised axle cornering stiffness front is exceeded by the normalised axle cornering stiffness aft.
4. A vehicle is understeered if the steering wheel gradient $\partial\delta/\partial a_y > 0$

coincide. Graphically, expression (5) can be plotted as shown in figure 11, referred to as the handling diagram (see [3]).

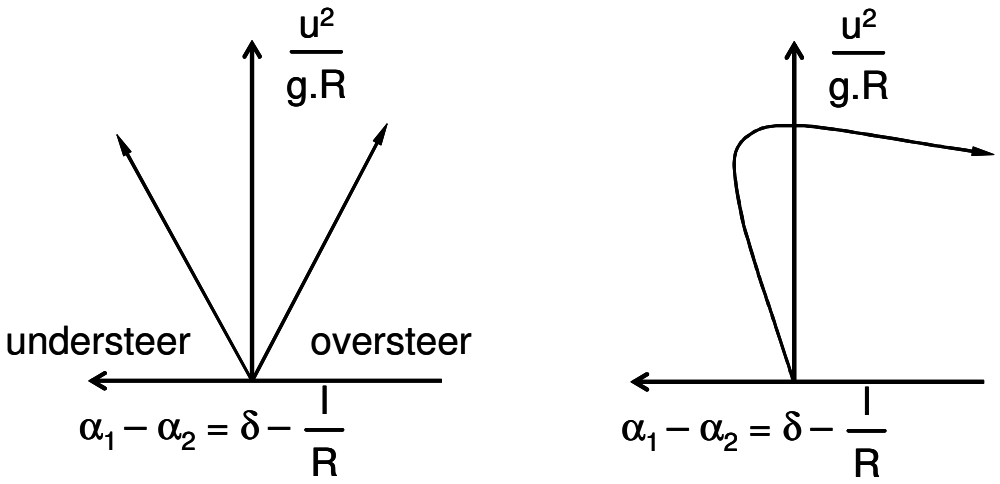

Figure 11. :The handling diagram for linear (left) and nonlinear (right) axle characteristics.

The left picture corresponds to linear axle characteristics. The right-hand picture is the extension to nonlinear axle characteristics (schematic) in case of a vehicle being understeered for small lateral acceleration, and restricted to positive steering angle. To explain this, we invert the normalized axle characteristics:

$$g_i(a_y) = inv[f_{yi}(\alpha_i)](a_y) \quad ; \text{i=1,2} \tag{7}$$

These functions g_i are multivalued functions in the lateral acceleration a_y (in g's, i.e. K/(mg)), where both single-valued branches may be treated separately.
It follows using (4) and (7) that:

$$\alpha_1 - \alpha_2 = \delta - \frac{l}{R} = g_1(a_y) - g_2(a_y) \equiv h(a_y) \tag{8}$$

This function $h(a_y)$ is directly related to the vehicle axle characteristics, and will therefore show different shapes for vehicles being initially (linear range) understeered or oversteered. Compare figure 12 where handling diagrams are plotted for two different sets of normalized axle characteristics. Observe the change in orientation of the handling curve for both cases.

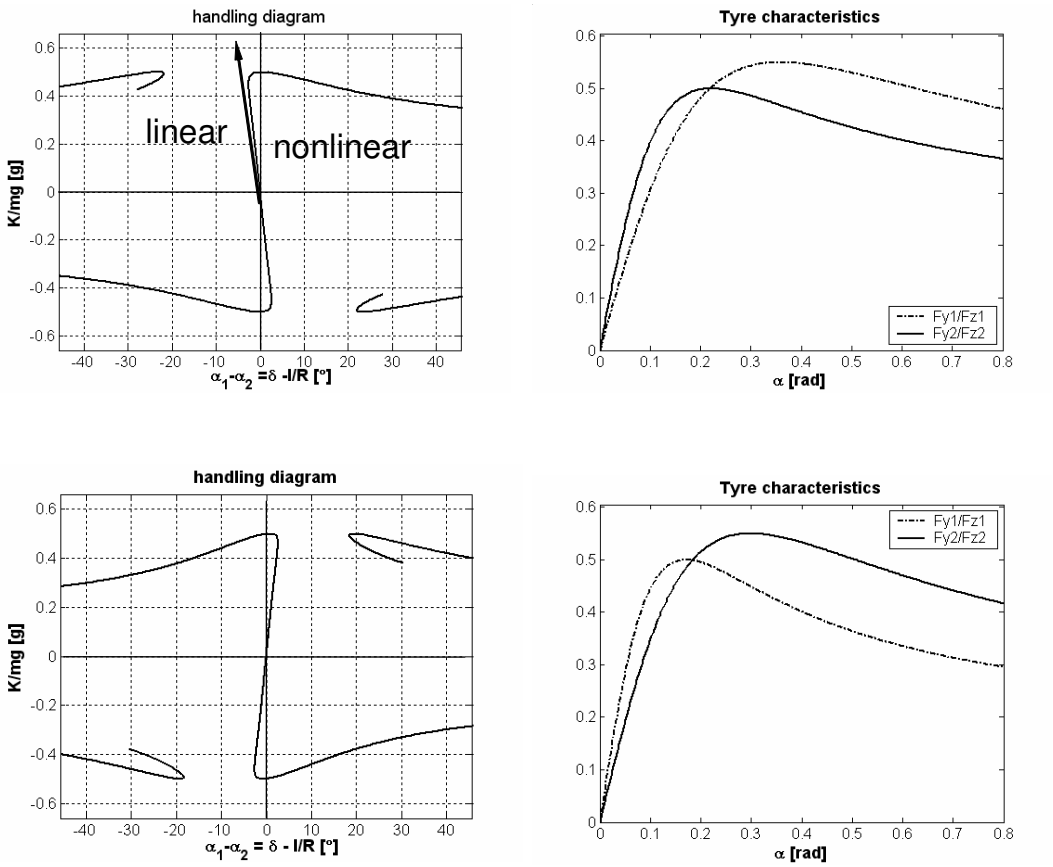

Figure 12. :Handling diagrams for different sets of axle characteristics.

Let's start with the upper left plot of figure 12. The corresponding axle characteristics were used to derive the phase plane plots in figure 4. Remember that we derived three different steady state solutions in this case. This diagram, referred to as part A of the handling diagram, will be merged with another diagram having the ordinate K/(mg), expressing this lateral acceleration in terms of path curvature l/R according to equation (5). That means that this second diagram, referred to as handling diagram-part B (a_y versus curvature), is a family of straight lines (u-lines) with the slope proportional to the square of the vehicle speed. According to (4) both diagrams combined produce the steering angle as the horizontal distance between handling curve and u-line. Both parts A and B are shown in figure 13, which we'll discuss here step by step.
Assume a path-radius R_1 (i.e. path curvature l/R_1) and a vehicle forward speed u_1. That means that the point (l/R, K/(mg)) is lying on the straight line with slope $(u_1^2/(g.l))$. Because of (4), applying a steering angle δ means that this u-line is shifted to the left over a horizontal distance δ.

As a result, the steady state solution I is found as the intersection of part A and the shifted u-line, and lying in the understeer region. For very small speed u, the corresponding straight line is almost coinciding with the horizontal axis, and consequently, the necessary steering angle to reach the origin equals l/R (the Ackermann angle). For the curve in figure 13 (similar to the curve in the left-top picture in figure 12) three steady state solutions arise, denoted as I, II and III as long as δ is not too large, confirmed by our earlier observation regarding the phase plane plot 4. For a certain value of δ, $\delta = \delta_S$ the point S is reached and beyond this value, the number of three steady state solutions drops down to 1. This situation corresponds with the case where too excessive steering yields instability.
Summarizing, the handling diagram relates the steady state solutions to input variables R(vertical lines in the right half of the handling diagram), steering angle δ (horizontal shift of the u-line), vehicle speed (u-lines) and the axle characteristics (the S-shaped curve, including the additional branches resulting from the fact that the functions g_i in (7) are multivalued). Clearly, these variables cannot be chosen independently.

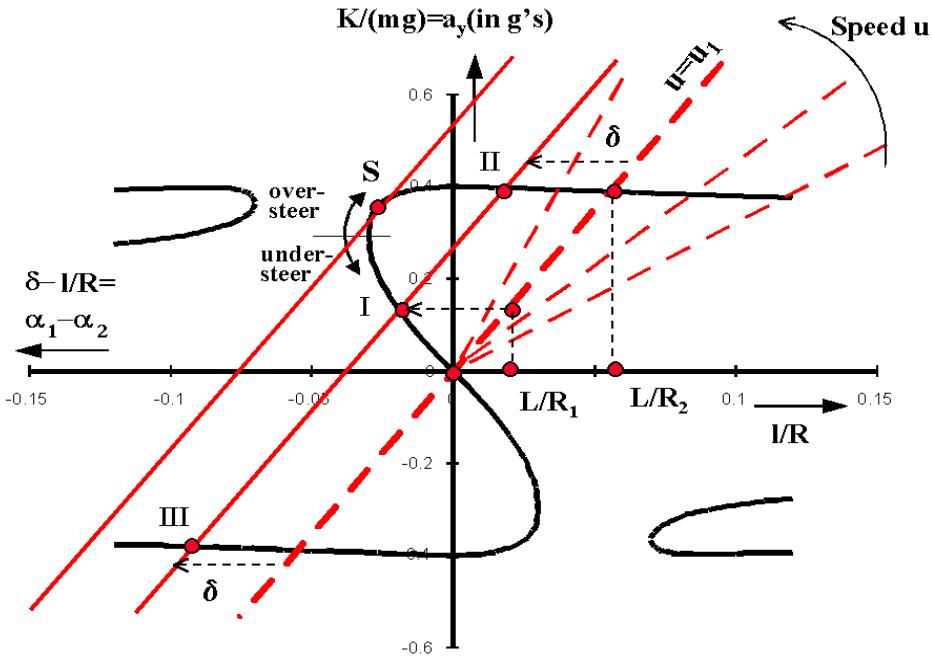

Figure 13.: Handling diagram in total, combining parts A and B (see text)

Now assume the steering angle δ to be chosen below δ_S but close to it, and consider the resulting steady state solution I. Slightly increasing the lateral acceleration a_y implies increase of the steering angle in order to reach a new steady state solution. That means that I is stable as long as it is situated below S. In the same way one may conclude that, for the steady state solution II lying above S, increase of a_y would involve reduction of steering angle δ yielding a self-reinforcing effect towards smaller curve radius and larger lateral acceleration, i.e. corresponding to yaw-instability.

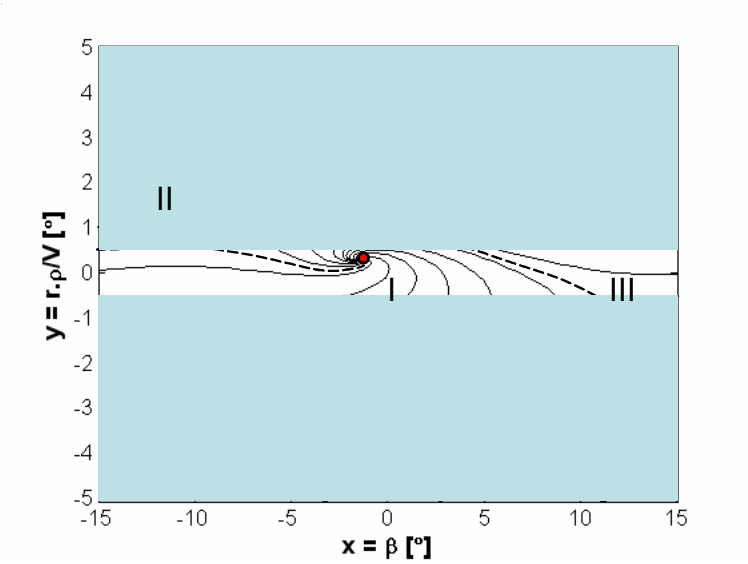

Figuur 14.: Energy phase plane, axle characteristics cf. figure 12 (top), with u = 75 km/h and δ = 1.5°

These results can be proved rigorously, i.e. solutions on the main branch become unstable as soon as the slope of the tangent to this curve in the solution point becomes smaller than the slope of the u-line (shifted over δ) concerned. This means that the path curvature where δ becomes maximal at the vehicle speed u considered has been exceeded. This kind of instability can only occur if the vehicle behaves oversteered, i.e. when the slope of the handling curve is positive. Decreasing of the speed u leads to increase of the lateral acceleration where the steering angle is maximal. Likewise, instability occurs in point III.

We have blown up the right-hand picture in figure 4 in figure 14, including all the three steady state points for some combination of vehicle speed and steering angle. One clearly observes some trajectories not approaching the stable steady state point. The dashed lines correspond to the so-called separatrices (manifolds), separating the solution curves approaching the unstable outmost steady state points, but never reaching them. On the other hand, all solution curves within the intermediate area approach these steady state conditions and determine the global stability of this point. Consequently, the unstable steady state points (points II and III in figure 13) determine the **domain of attraction** of steady state point I

4. STABILITY DIAGRAM

This section will focus further on the stability of steady state points in relationship to the slope of the normalized axle characteristics, at the steady state values for the slip angles α_1 and α_2, respectively.
Let us return to the set of equations in its general form:

$$\frac{d\,\underline{y}}{dt} = F(\underline{y}) \;\; ; t > 0$$

Steady state solutions satisfy

$$F(\underline{y}_0) = 0$$

These steady state solutions are points in the (energy) phase plane as introduced in section 2, denoted as equilibrium points or **singular points**, since the time derivatives of both y_1 and y_2 vanish in these points. In terms of the phase plane, one observes trajectories that move away, form closed cycles or approach these singular points, respectively.
Under mild conditions one can prove that, near such a singular point, the solutions of the non-linear system show the same qualitative behaviour as solutions of the linearised system around these points:

$$\frac{d\,\underline{y}}{dt} = F'(\underline{y}_0).(\underline{y} - \underline{y}_0) \;\; ; t > 0$$

with Jacobian matrix $F'(\underline{y}_0)$. It follows that the behaviour near a singular point can be determined from the knowledge of the eigenvalues of this Jacobian matrix. These eigenvalues, denoted as λ_1, λ_2 are either real or complex conjugated. The possible shapes of the singular points are summarized in figure 16. Except for the saddle point and the centre, each type may be connected to a stable steady state points (trajectories moving towards this point) or an unstable steady state point (trajectories moving away from this point).

Saddle points correspond to unstable stationary solutions, since trajectories may pass this point at close distance, but then move away never to return. Nodes and stars correspond to solutions where the stationary conditions may be approached in a nonoscillatory (i.e. overdamped) way. On the other hand, a focus means oscillatory (i.e. underdamped) performance. Compare with figure 7, where a ramp steer steering input is followed by an oscillatory yaw behaviour approach a steady state cornering situation. This is a typical vehicle behaviour for most

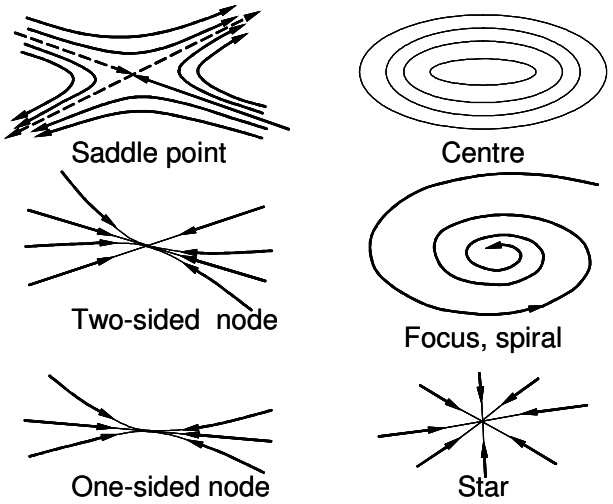

Figure 15.: Possible shapes singular points

understeered vehicles with not too low speed. One recognises the stable focus and the two unstable saddle points in figure 14, and the stable two-sided (two-tangent) node in figure 9.

Figure 16 shows the time history of the yawrate for a ramp steer input for the case of normal understeer, understeer for low speed, and stable oversteer, respectively. Only for the first choice of vehicle input and axle characteristics, one observes an overshoot, i.e. a stable focus in the phase plane. In both other situations, the yawrate approaches the steady state value in a monotonous way, corresponding to a node.

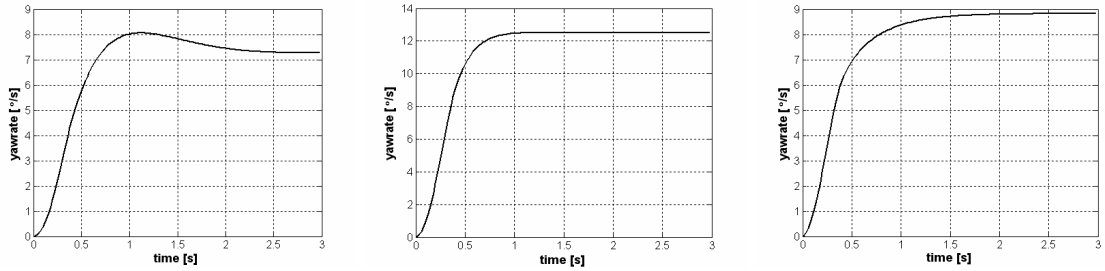

Figure 16.: Yawrate vs. time for axle characteristics cf. figure 12 (top: first two plots, bottom: last plot, for (u, δ) = (80 km/h, 1.5°), (35 km/h, 4°) and (30 km/h, 2°), respectively)

Stationary solutions are related to the axle slipangles for which the normalized axle characteristics coincide (see figure 17 for an example) and (4) is satisfied. The types of singular point as shown in figure 15 depend on the slope of the normalized axle characteristics at these slipangles, and one may derive the diagram shown in figure 18, referred to as the **stability diagram**. Both positive and negative values of these slopes are included in this diagram where, obviously, only small negative values are realistic (indicated with a box).
A remarkable symmetry is apparent in this diagram. Two hyperbolic curves separate the regions where stationary points are saddle points and where they

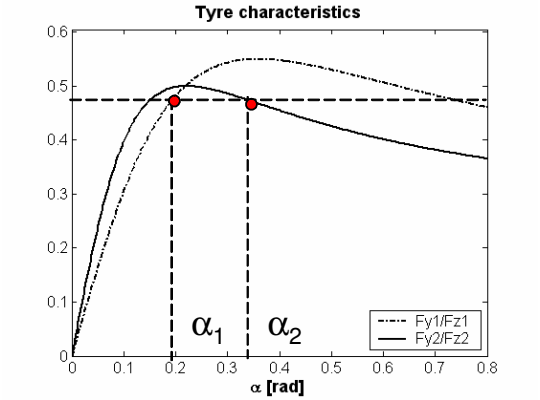

Figure 17.: Normalized axle characteristics coincide under steady state conditions.

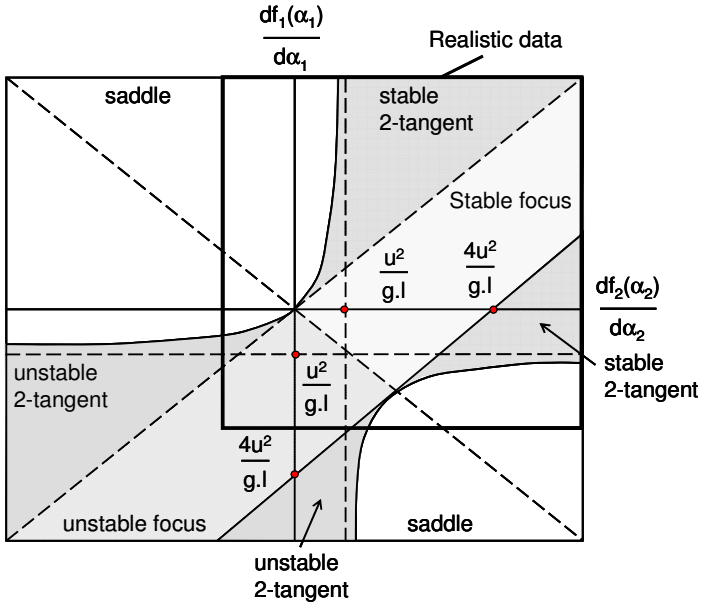

Figure 18.: The Stability Diagram

are nodes. Above the diagonal from bottom right to top left, these nodes are stable, whereas below this diagonal, these nodes are unstable.
A band in between (from bottom left to top right) contains the oscillatory singular points, with the stable points above the diagonal referred to earlier. The hyperbolic curves depend on the ratio of speed and acceleration of gravity times wheelbase. Hence, reducing speed means that points in the 'focusarea' may end up in the 'node area', as we observed before in figure 16.
Let us consider the first quadrant. The lower half (the first octant) corresponds with the normal understeer behaviour, apparently consisting of a part with oscillatory behaviour near the steady

state solution and a part with monotonous approaching solution curves. The second octant consists of two parts also, with the shaded part being the stable region and the nonshaded part corresponding to instability. Indeed, with the speed decreasing, the shaded region expands demonstrating the improved stability. Note that there also exists a stable region in the fourth quadrant, again consisting of a 'focus-region' and a 'node region'. This stable region corresponds with the case of excessive understeer, where the vehicle speed needs to exceed a certain minimum value to guarantee stability.

5. DISCUSSION ON VISUALIZATION TOOLS

In the preceding sections, we have reviewed existing graphical tools and introduced a new one to visualize the fundamental vehicle handling performance in relationship to vehicle parameters and nonlinear axle (tyre) characteristics. How can it help us in such dynamic handling analyses, especially when we are faced with more complex simulation models?
Important is the performance near steady state conditions. Think about special manoeuvres as a vertical disturbance during cornering, a ramp steer input, etc. A first step might be to plot the solution curve in the energy phase plane. This already gives an understanding near the stationary points, the performance in terms of drifting and spinning, and the varying position of the momentary pole of rotation (rotation length). Manoeuvring for varying vehicle design parameters leads to different trajectories and therefore different an interpretation of the impact of these variations on handling performance along the guidelines as discussed in section 2.
The handling diagram can be derived from the steady state testresults up to the limit behaviour (steering angle versus lateral acceleration) or directly from the nonlinear axle characteristics. Variation of curvature, speed, steering angle, axle characteristics leads to different stationary solutions which can be derived from this handling diagram. Also the (local and global) stability can be discussed from this diagram.
Finally, the stability diagram tells us if and why the performance near the stationary conditions is oscillatory or not, if it is stable or unstable, and to what extent this is effected by the vehicle speed.

The tools will help the vehicle engineer to separate the basic fundamental vehicle performance from the higher order dynamic vehicle results.

REFERENCES

[1]. K-H Guo: A *Study of a Phase Plane Representation for Identifying Vehicle Behavior.* Proceedings of the 9th IAVSD Symposium, Linköping (1985)

[2]. H.B. Pacejka.: Tyre Factors and Vehicle Handling. International Journal of Vehicle Design. Vol. 1 (1979)

[3]. H.B. Pacejka.: Tyre and Vehicle Dynamics. Butterworth Heinemann (2002).

[4]. H. K. Sachs, M.Singh.: *Automobile Stability – A Study of the Domains of Attraction. The Dynamics of Vehicles on Roads and Tracks.* Proceedings 5th VSD Symposium, Vienna (1997)

[5]. H.T. Smakman.: *Functional Integration of Slip Control with Active Suspension for Improved Lateral Vehicle Dynamics.* Thesis Delft University of Technology (2000)

[6]. C. Winkler.: *Simplified Analysis of the Steady-State Turning of Complex Vehicles*. Vehicle System Dynamics, 29 (1998)